Electronic Supplementary Information

Experimental Section

Materials: Potassium fluosilicate (K_2SiF_6), nickel nitrate hexahydrate ($Ni(NO_3)_2·6H_2O$), iron nitrate nonahydrate ($Fe(NO_3)_3·9H_2O$), sodium hydroxide (NaOH), potassium hydroxide (KOH), and N, N-diethyl-p-phenylenediamine (DPD) were sourced from Shanghai Maclin Biochemical Technology Co., Ltd. Ammonium fluoride (NH_4F), urea ($CO(NH_2)_2$), sodium carbonate (Na_2CO_3), sodium chloride (NaCl), ruthenium oxide (RuO_2), and nafion (5 wt.%) were acquired from Aladdin Ltd. (Shanghai, China). Hydrochloric acid (HCl), potassium permanganate ($KMnO_4$), sulfuric acid (H_2SO_4), and ethanol (C_2H_5OH) were obtained from the Chengdu Kelong Chemical Reagent Factory. The Ni foam used in this study was bought from Qingyuan Metal Materials Co., Ltd (Xingtai, China). Ultrapure water was used throughout the experiments.

Preparation of NiFe LDH/NF and SiF_6^{2-}-NiFe LDH/NF: Firstly, NF with a size of 2.0 cm × 3.0 cm was sonicated in 3 M HCl, ethanol, and deionized water, respectively for 15 min. Meanwhile, 1 mmol $Fe(NO_3)_3·9H_2O$, 2 mmol $Ni(NO_3)_2·6H_2O$, 1 mmol urea, and 4 mmol NH_4F were mixed with 35 mL of deionized water and stirred for 20 minutes at room temperature to obtain a precursor solution. Subsequently, the precursor solution was transferred into a Teflon-lined autoclave along with the pre-treated NF, the autoclave was sealed and maintained at 120 °C for 6 h in an oven and cooled down to room temperature naturally. Then the as-prepared sample was washed thoroughly with deionized water and ethanol several times and dried at 60 °C for 30 min in air. The final sample obtained was NiFe LDH/NF. The SiF_6^{2-}-NiFe LDH/NF was prepared by simple immersion. The NiFe LDH/NF was immersed in 0.05 mM K_2SiF_6 aqueous solution for several minutes. After several washes with DI water and drying at 60 °C, SiF_6^{2-}-NiFe LDH/NF was obtained.

Preparation of RuO_2/NF or Pt/C/NF: An ethanol solution (with a 50/50 vol split of water and ethanol) and an extra 30 μL of Nafion binder were employed to disperse RuO_2 (or 20% Pt/C) powder for the ink (5 mg mL^{-1}). The resulting ink in a small

centrifuge tube underwent approximately 30 min of sonication, followed by the pipette transfer of 100 μL of the ink dropwise onto a cleaned NF. The electrode was then fabricated after drying.

Characterizations: X-ray diffraction (XRD) patterns were acquired on Shimadzu XRD-6100 S2 diffractometer with Cu-K radiation at a scanning speed of 5° $minute^{-1}$. Raman spectroscopy was recorded on the Lab RAM HR Evolution confocal microscope with 532 nm laser. The morphology and structure of the synthesized samples were examined via SEM (Zeiss Gemini SEM 300) and TEM (FEI TF200). Chemical compositions and element distributions were analyzed using the ESCALABMK II X-ray photoelectron spectrometer system and EDX mapping. Absorbance measurements were conducted with a UV-vis spectrophotometer (Shimadzu UV-2700). The elemental composition was determined by Inductively Coupled Plasma-Optical Emission Spectroscopy (ICP-OES, SPECTRO ARCOS II MV, Germany).

Electrochemical measurements: All electrochemical experiments were conducted utilizing a CHI660 analyzer (CH Instruments, Inc., Shanghai). The experiments employed the standard three-electrode configuration, a graphite rod acted as the counter electrode, the prepared samples as the working electrode, and an Hg/HgO electrode served as the reference electrode. Linear sweep voltammetry (LSV) curves were obtained over a potential range of 0 to 1.4 V with a scan rate of 5 mV s^{-1}. Potentials were standardized to the reversible hydrogen electrode (RHE) scale using the formula: E (RHE) =E (Hg/HgO) + 0.098 + 0.059 × pH. The iR-compensated potential was derived by using the equation: E_{corr} =E – iR, with E being the original potential, R the solution resistance, i the current, and Ecorr the iR-compensated potential. The double-layer capacitance (C_{dl}) values were assessed through cyclic voltammetry (CV) at a scan rate from 20 to 100 mV s^{-1} in alkaline freshwater.

Determination of active chlorine: UV-vis spectrophotometer was utilized to determine the concentration of active chlorine in the electrolyte through the DPD colorimetric method. After the long-term stability test at 1000 mA cm^{-2}, DPD was

added to the electrolyte, causing a pink coloration. UV-vis absorption spectrometry at 550 nm was used to analyze different active chlorine concentrations.

Computational details: In our calculations, both the AEM and LOM mechanisms were considered to achieve a better understanding of the oxygen evolution reaction (OER) processes. The analysis of the AEM mechanism proceeded through four steps:

$* + H_2O \rightarrow *OH + H^+ + e^-$

$*OH \rightarrow *O + H^+ + e^-$

$*O + H_2O \rightarrow *OOH + H^+ + e^-$

$*OOH \rightarrow * + O_2(g) + H^+ + e^-$

where * denotes the catalysis surface.

And the LOM mechanism was analyzed through four additional steps:

$*OH \rightarrow *O_l + H^+ + e^-$

$*O_l + H_2O \rightarrow *OOH + H^+ + e^-$

$*OOH \rightarrow *OO + H^+ + e^-$

$*OO \rightarrow O_2(g) + O_v + e^-$

where O_l represents lattice oxygen and O_v represents oxygen vacancy.

The Gibbs free energy change in each step was calculated by:

$\Delta G = \Delta E + \Delta ZPE - T\Delta S$

where ΔG is the change of Gibbs free energy. ΔE is the change of energy obtained from DFT calculations. ΔZPE and $T\Delta S$ are the corrections for zero point energy and entropy, respectively. The theoretical overpotentials (η) were calculated by:

$\eta = \Delta G_{max} - 1.23$ V

where ΔG_{max} is the maximum free energy change in the OER process.

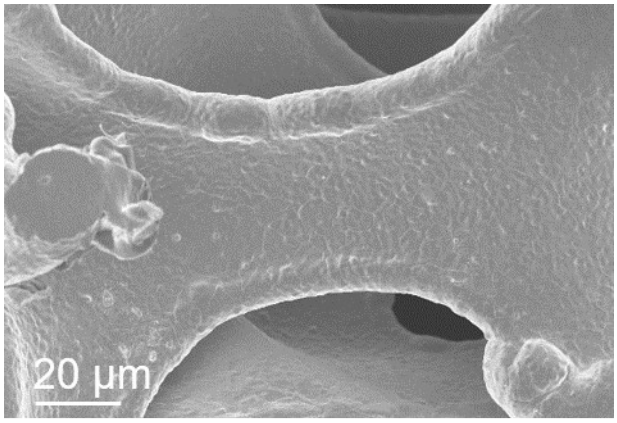

Fig. S1. SEM image of bare NF.

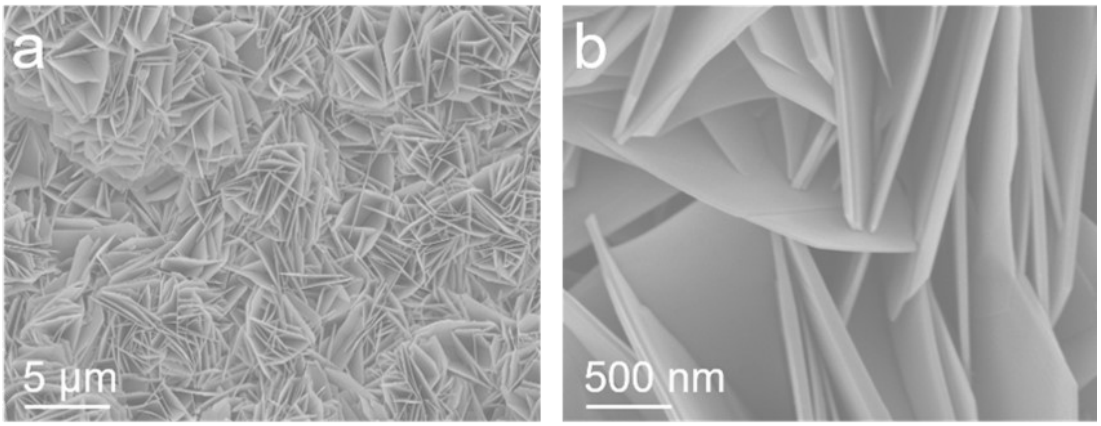

Fig. S2. (a) Low- and (b) high-magnification SEM images of NiFe LDH/NF.

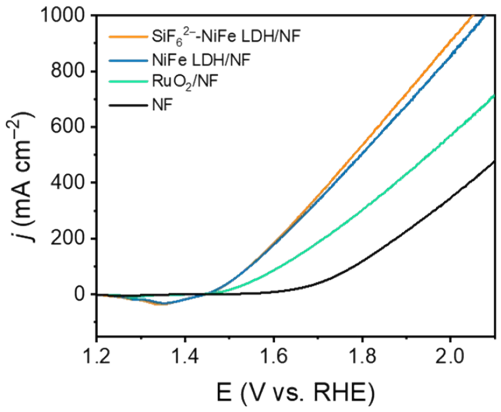

Fig. S3. LSV curves of different electrocatalysts in 1 M KOH without iR compensation.

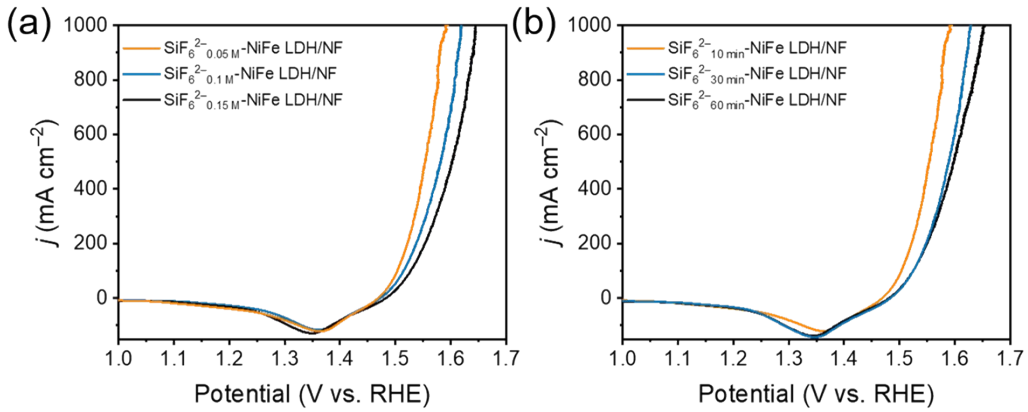

Fig. S4. LSV curves of different Na_2SiF_6 (a) concentrations and (b) immersion times in 1 M KOH.

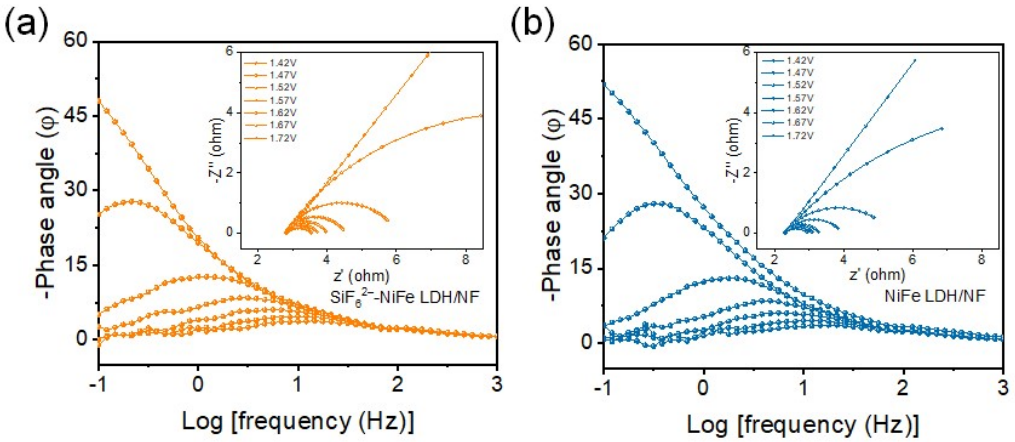

Fig. S5. Operando Nyquist plots and the corresponding Bode plots of (a) SiF_6^{2-}-NiFe LDH/NF and (b) NiFe LDH/NF at different potential versus RHE.

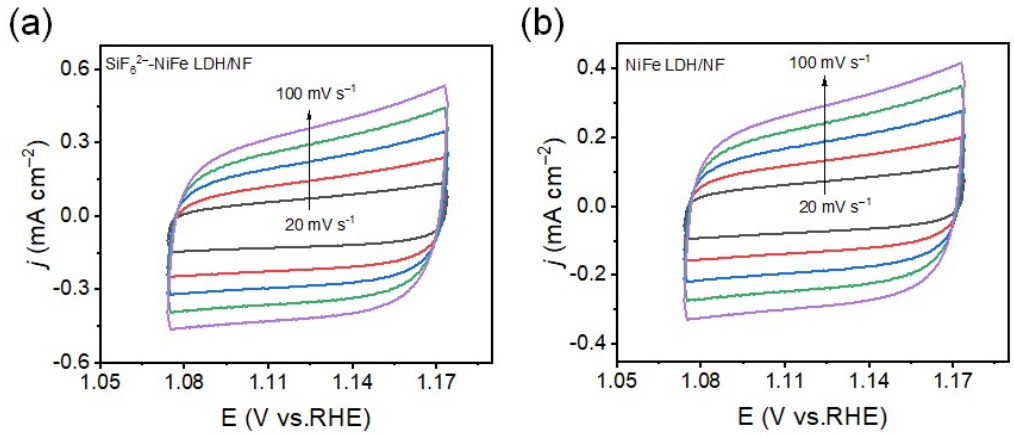

Fig. S6. CV curves of (a) SiF_6^{2-}-NiFe LDH/NF and (b) NiFe LDH/NF in the double layer region at different scan rates of 20, 40, 60, 80, and 100 mV s^{-1} in 1 M KOH.

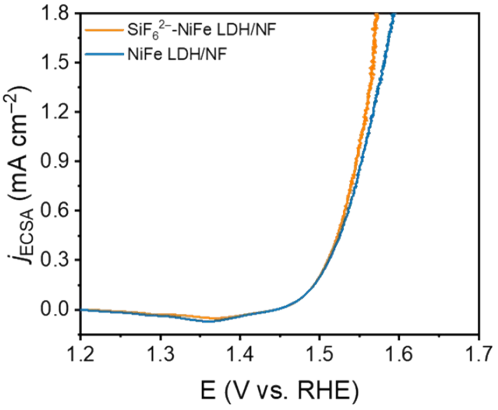

Fig. S7. ECSA-normalized LSV curves of SiF_6^{2-}-NiFe LDH/NF and NiFe LDH/NF.

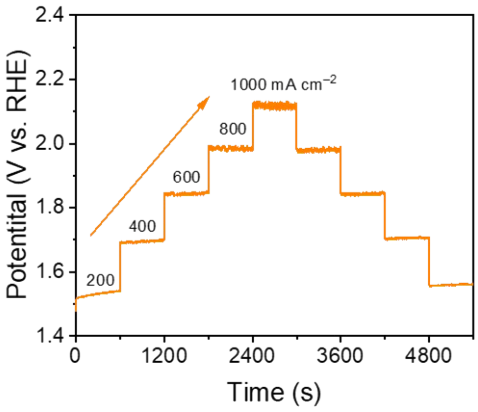

Fig. S8. Multistep chronopotentiometric curves of SiF_6^{2-}-NiFe LDH/NF without iR correction 1 M KOH.

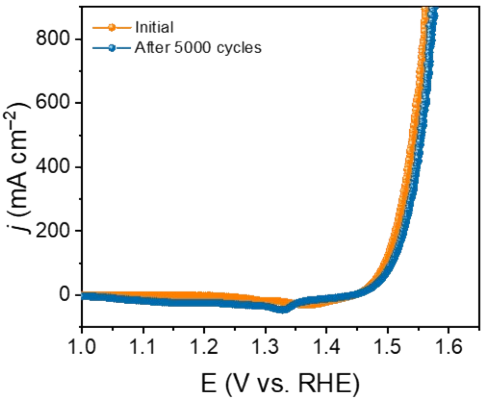

Fig. S9. LSV curves of SiF_6^{2-}-NiFe LDH/NF before and after 5000 CV cycles in 1 M KOH.

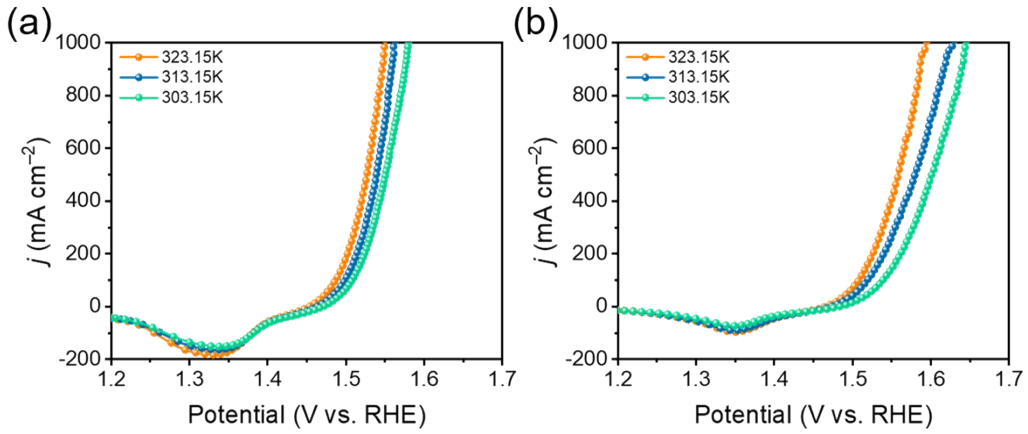

Fig. S10. LSV curves of (a) SiF_6^{2-}-NiFe LDH/NF and (b) NiFe LDH/NF toward OER at different temperatures.

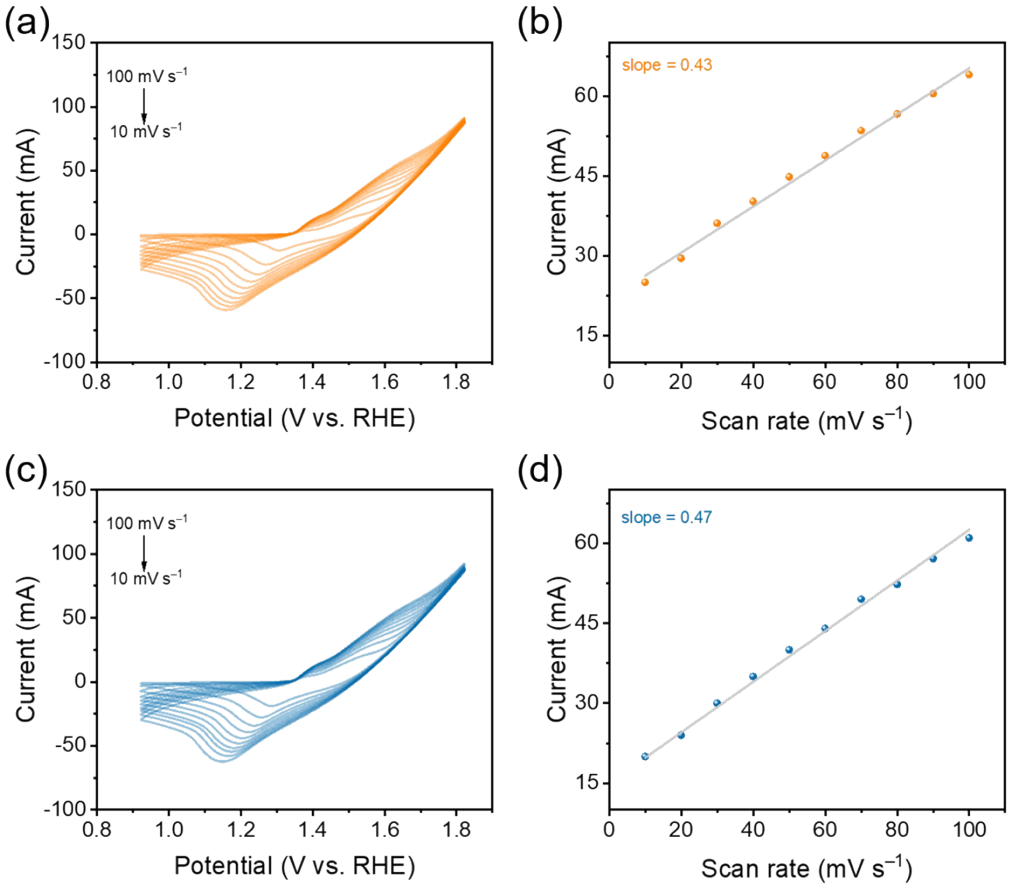

Fig. S11. CV curves of (a) SiF_6^{2-}-NiFe LDH/NF and (c) NiFe LDH/NF at different scan rates increasing from 10 to 100 mV s^{-1} in 1 M KOH. Oxidation peak current versus the scan rate plot of (b) SiF_6^{2-}-NiFe LDH/NF and (d) NiFe LDH/NF.

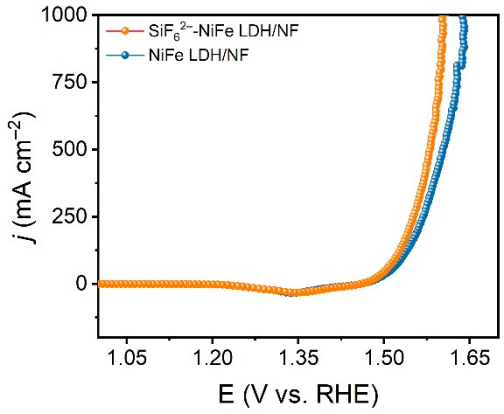

Fig. S12. LSV curves of SiF_6^{2-}-NiFe LDH/NF and NiFe LDH/NF in 1 M KOH + seawater.

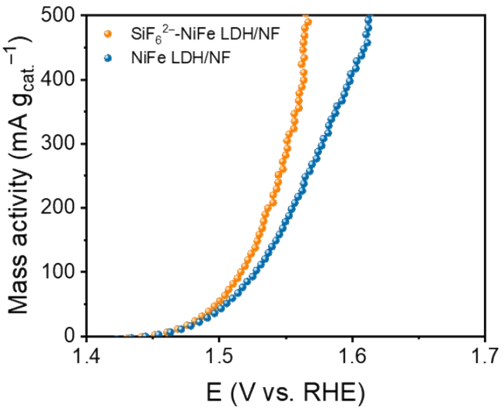

Fig. S13. Mass activity curves of SiF_6^{2-}-NiFe LDH/NF and NiFe LDH/NF.

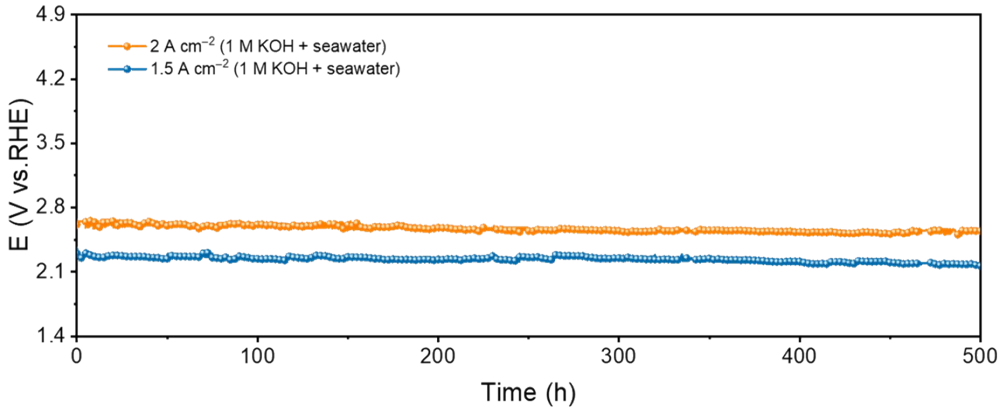

Fig. S14. Chronopotentiometry curves of SiF_6^{2-}-NiFe LDH/NF at 1.5 and 2 A cm^{-2} without iR correction in 1 M KOH + seawater.

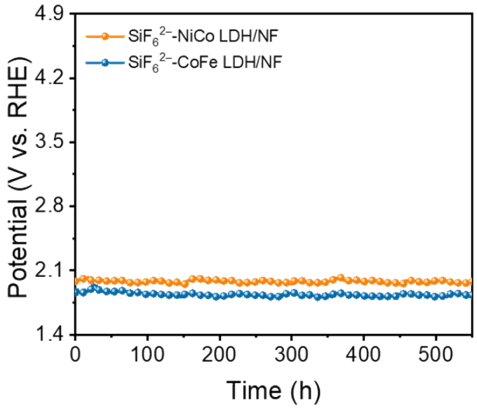

Figure S15. Chronopotentiometry curves of SiF_6^{2-}-NiCo LDH/NF and SiF_6^{2-}-CoFe LDH/NF at 1000 mA cm^{-2} without iR correction in 1 M KOH + seawater.

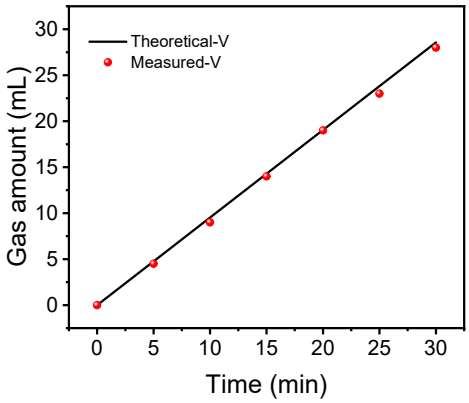

Fig. S16. Comparison between the amount of collected and theoretical O_2 for SiF_6^{2-}-NiFe LDH/NF at a *j* of 1000 mA cm^{-2} in 1 M KOH + seawater.

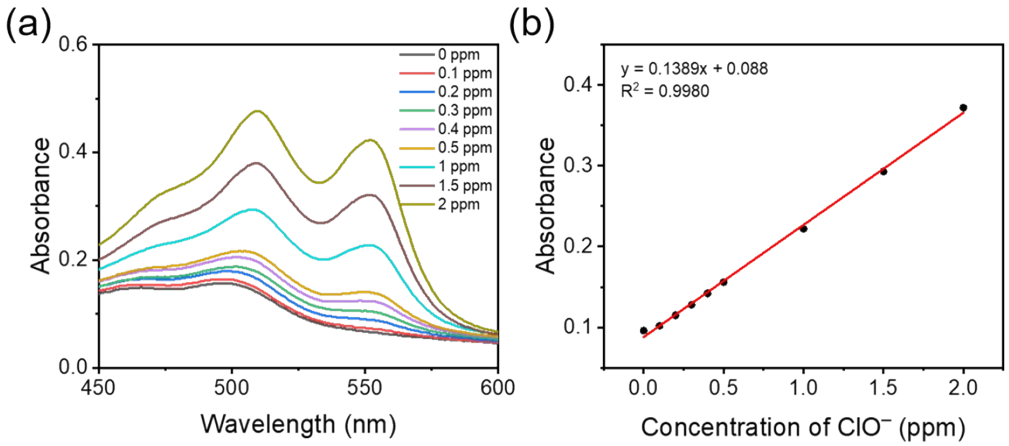

Fig. S17. (a) UV-vis absorption spectra of various active chlorine concentrations. (b) Calibration curve was used to evaluate ClO^- concentrations of the electrolyte.

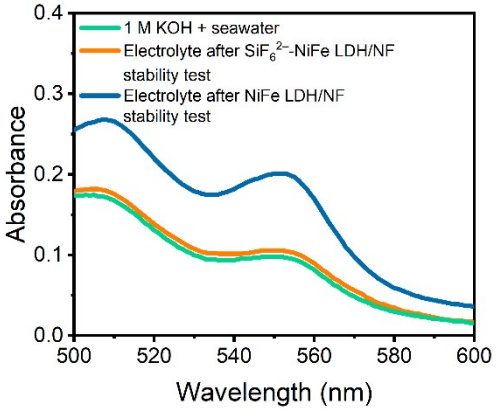

Fig. S18. UV-vis absorption spectra of the collected electrolytes from SiF_6^{2-}-NiFe LDH/NF and NiFe LDH/NF stability test at 1000 mA cm^{-2}.

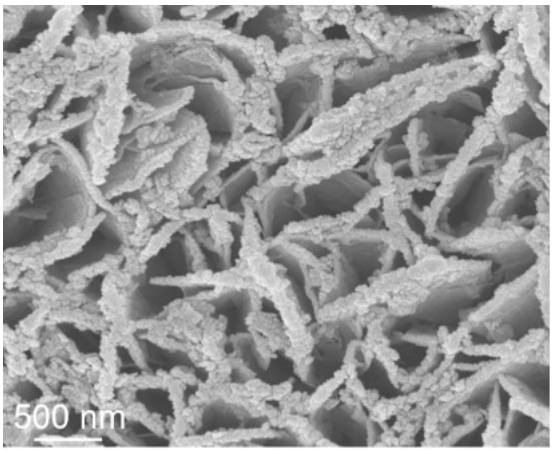

Fig. S19. SEM image of SiF_6^{2-}-NiFe LDH/NF after durability test in 1 M KOH + seawater.

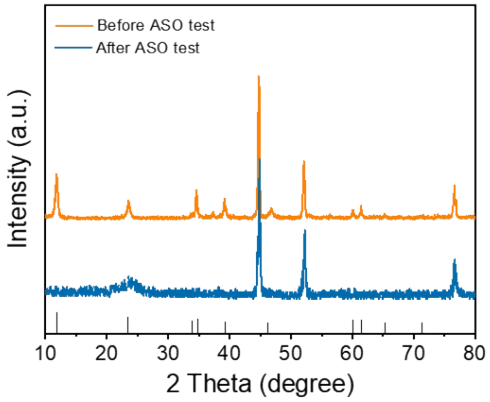

Fig. S20. XRD patterns of SiF_6^{2-}-NiFe LDH/NF before and after OER stability test in 1 M KOH + seawater.

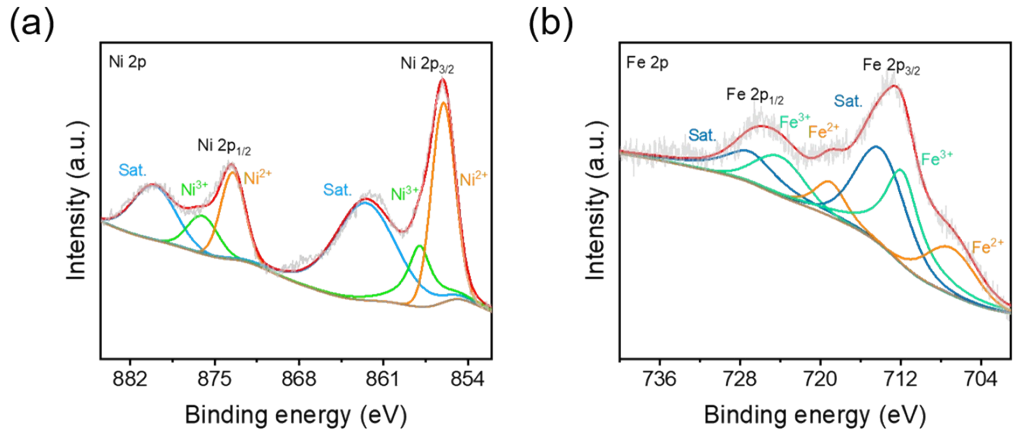

Fig. S21. XPS spectra of SiF_6^{2-}-NiFe LDH in the (a) Ni 2p and (b) Fe 2p regions after OER stability test in 1 M KOH + seawater.

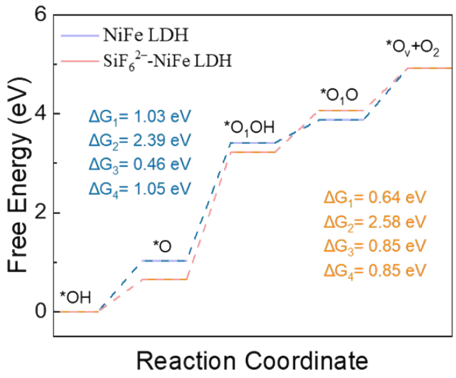

Fig. S22. Free energy diagrams of LOM in SiF_6^{2-}-NiFe LDH and NiFe LDH.

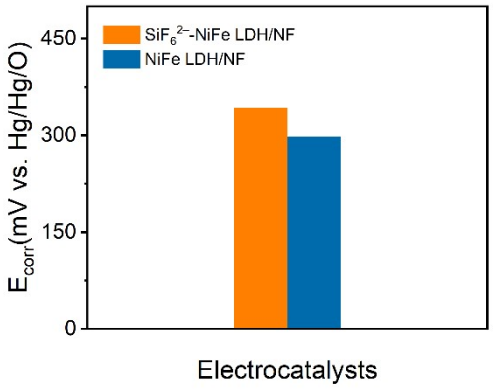

Fig. S23. Corrosion potentials of SiF_6^{2-}-NiFe LDH/NF and NiFe LDH/NF electrodes in 1 M KOH + seawater.

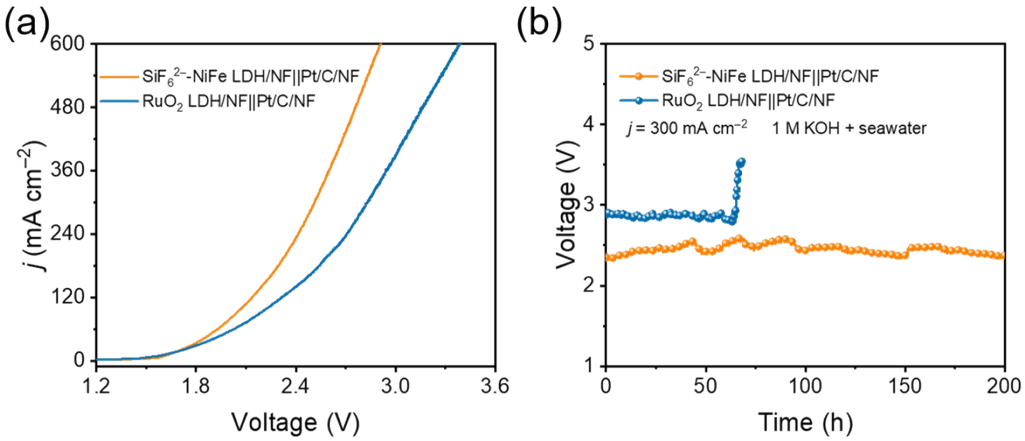

Fig. S24. (a) The AEM-based electrolysis performance of SiF_6^{2-}-NiFe LDH/NF||Pt/C/NF and RuO_2/NF||Pt/C/NF pairs in 1 M KOH + seawater. (b) Chronopotentiometry curves of SiF_6^{2-}-NiFe LDH/NF||Pt/C/NF and RuO_2/NF||Pt/C/NF in 1 M KOH + seawater.

Table S1 EIS parameters of the samples.

Catalyst	R_s/Ω	R_{ct}/Ω
SiF_6^{2-}-NiFe LDH/NF	2.22	3.28
NiFe LDH/NF	2.72	4.27

R_s: solution resistance.
R_{ct}: charge transfer resistance.

Table S2 Comparison of OER catalytic performance for seawater oxidation of SiF_6^{2-}-NiFe LDH/NF with recent reported catalysts.

Catalysts	Current Density (mA cm^{-2})	Overpotential (mV)	Electrolyte	Ref.
SiF_6^{2-}-NiFe LDH/NF	500	350	1 M KOH + seawater	This work
	1000	371	1 M KOH + seawater	
MnCo/NiSe/NF	500	419	1 M KOH + seawater	1
	1000	460	1 M KOH + seawater	
NiFeO-CeO_2/NF	500	338	1 M KOH + seawater	2
	1000	408	1 M KOH + seawater	
Ni_3S_2/Co_3S_4/NF	500	440	1 M KOH + seawater	3
S-Ni/Fe(OOH)/NF	100	300	1 M KOH + seawater	4
	500	398	1 M KOH + seawater	
Ni_2P-Fe_2P/NF	100	305	1 M KOH + seawater	5
	1000	431	1 M KOH + seawater	
Cr-CoCH/NF	100	394	1 M KOH + seawater	6
NiMoN@NiFeN/NF	500	369	1 M KOH + seawater	7
Fe-NiS/NF	500	377	1 M KOH + seawater	8
	1000	420	1 M KOH + seawater	
$Ni(OH)_2$-TCNQ/GP	100	382	1 M KOH + seawater	9
Ir@NiFe-MOF/NF	1000	500	1 M KOH + seawater	10
NiCoHPi@Ni_3N/NF	500	474	1 M KOH + seawater	11
(Ni/Fe/Mo)OOH/NF	500	520	1 M KOH + seawater	12

$NiSe_2$@NiOOH/NF	100	360	1 M KOH + seawater	13
	500	460	1 M KOH + seawater	

Table S3. Element analysis of SiF_6^{2-}-NiFe LDH/NF after stability test by ICP-MS.

Element	Element concentrat1on (ppm)
Ni	0.034
Fe	0.075
Si	0.005

Table S4. Element analysis of NiFe LDH/NF after stability test by ICP-MS.

Element	Element concentrat1on (ppm)
Ni	0.045
Fe	0.097

References

1 R. Andaveh, A. S. Rouhaghdam, J. Ai, M. Maleki, K. Wang, A. Seif, G. B. Darband and J. Li, *Appl. Catal. B Environ.*, 2023, **325***,* 122355.

2 H. Zhang, Z. Bi, P. Sun, A. Chen, T. Wågberg, X. Hu, X. Liu, L. Jiang and G. Hu, *ACS Nano*, 2023, **17**, 16008–16019.

3 C. Wang, M. Zhu, Z. Cao, P. Zhu, Y. Cao, X. Xu, C. Xu and Z. Yin, *Appl. Catal. B Environ.*, 2021, **291**, 120071.

4 L. Yu, L. Wu, B. McElhenny, S. Song, D. Luo, F. Zhang, Y. Yu, S. Chen and Z. Ren, *Energy Environ. Sci.*, 2020, **13**, 3439–3446.

5 L. Wu, L. Yu, F. Zhang, B. McElhenny, D. Luo, A. Karim, S. Chen and Z. Ren, *Adv. Funct. Mater.*, 2021, **31**, 2006484.

6 M. Zhang, X. He, K. Dong, H. Zhang, Y. Yao, C. Yang, M. Yue, S. Sun, Y. Sun, D. Zheng, Y. Luo, Q. Liu, N. Li, B. Tang, J. Liu and X. Sun, *Chem. Commun.*, 2023, **59**, 9750–9753.

7 L. Yu, Q. Zhu, S. Song, B. McElhenny, D. Wang, C. Wu, Z. Qin, J. Bao, Y. Yu, S. Chen and Z. Ren, *Nat. Commun.*, 2019, **10**, 5106.

8 C. Yang, K. Dong, L. Zhang, X. He, J. Chen, S. Sun, M. Yue, H. Zhang, M. Zhang, D. Zheng, Y. Luo, B. Ying, Q. Liu, A. M. Asiri, M. S. Hamdy and X. Sun, *Inorg. Chem.*, 2023, **62**, 7976–7981.

9 L. Zhang, J. Wang, P. Liu, J. Liang, Y. Luo, G. Cui, B. Tang, Q. Liu, X. Yan, H. Hao, M. Liu, R. Gao and X. Sun, *Nano Res.*, 2022, **15**, 6084–6090.

10 J. Yang, Y. Wang, J. Yang, Y. Pang, X. Zhu, Y. Lu, Y. Wu, J. Wang, H. Chen, Z. Kou, Z. Shen, Z. Pan and J. Wang, *Small*, 2022, **18**, 2106187.

11 H. Sun, J. Sun, Y. Song, Y. Zhang, Y. Qiu, M. Sun, X. Tian, C. Li, Z. Lv and L. Zhang, *ACS Appl. Mater. Interfaces*, 2022, **14**, 22061–22070.

12 L. Xu, Y. Dong, W. Xu and W. Zhang, *Catalysts*, 2023, **13**, 924.

13 H. Zhang, X. He, K. Dong, Y. Yao, S. Sun, M. Zhang, M. Yue, C. Yang, D. Zheng, Q. Liu, Y. Luo, B. Ying, S. Alfaifi, X. Ji, B. Tang and X. Sun, *Mater. Today Phys.*, 2023, **38**, 101249.